Room-Temperature Mechanical Resonator with a Single Added or Subtracted Phonon

Rishi N. Patel, Timothy P. McKenna, Zhaoyou Wang, Jeremy D. Witmer, Wentao Jiang, Raphaël Van Laer, Christopher J. Sarabalis, and Amir H. Safavi-Naeini

Phys. Rev. Lett. **127**, 133602 — Published 20 September 2021

DOI: 10.1103/PhysRevLett.127.133602

Room-temperature Mechanical Resonator with a Single Added or Subtracted Phonon

Rishi N. Patel,* Timothy P. McKenna, Zhaoyou Wang, Jeremy D. Witmer, Wentao Jiang, Raphaël Van Laer, Christopher J. Sarabalis, and Amir H. Safavi-Naeini†
Ginzton Laboratory, Stanford University Department of Applied Physics

A room-temperature mechanical oscillator undergoes thermal Brownian motion with an amplitude much larger than the amplitude associated with a single phonon of excitation. This motion can be read out and manipulated using laser light using a cavity-optomechanical approach. By performing a strong quantum measurement, *i.e.*, counting single photons in the sidebands imparted on a laser, we herald the addition and subtraction of single phonons on the 300 K thermal motional state of a 4 GHz mechanical oscillator. To understand the resulting mechanical state, we implement a tomography scheme and observe highly non-Gaussian phase-space distributions. Using a maximum likelihood method, we infer the density matrix of the oscillator and confirm the counter-intuitive doubling of the mean phonon number resulting from phonon addition and subtraction.

A mechanical oscillator at room temperature will behave in nearly perfect accordance with the laws of classical statistical physics. Nonetheless, interaction with optical-frequency photons can lead to behaviour that is nonclassical. For the mechanical motion of trapped ions, laser cooling and coupling of motion to the internal electronic degrees of freedom has long been pursued as a path to realizing a scalable quantum computer [1]. For solid-state mechanical devices, the signatures of quantum noise and back-action have been observed at room temperature and proposed as a means to realize quantum sensors [2, 3]. A key feature of such optomechanical devices is their ability to efficiently generate correlations between motion and light [4]. A strong quantum measurement of the resulting light field, e.g, by using a single-photon detector can consequently alter the state of the mechanical system [5–10].

Experiments in nonlinear optics have shown that adding or subtracting photons fundamentally alters the state of an optical degree of freedom. For example, in photon addition, parametric down conversion followed by post-selection of an idler photon allows the preparation of a single-photon state from vacuum [11]. Photon subtraction, when operating on squeezed light is used to generate and enlarge Schrödinger's cat states [12, 13]. Both photon addition and subtraction are essential for a number of tasks in continuous variable quantum information processing, in which non-Gaussian states are often required [14]. Highly thermal states of light have also been converted to non-classical states by the addition of one photon [15–18] and even allowed a direct test of quantum commutation relations [19, 20].

Mechanical oscillators have emerged as an important avenue for realizing quantum technologies [21–24]. In contrast to previous work on cryogenically cooled devices, we perform experiments on a mechanical oscillator in a highly thermal state at room temperature, and use its interaction with optical photons to perform quantum-limited read-out and state control. First, we use single photon counting to prepare phonon-added and subtracted mechanical states in a regime where $kT \gg \hbar\omega_{\mathrm{m}}$. Second, building on tomography techniques in quantum optics [11, 14, 25, 26] and optomechanics [27, 28], we combine heralded single-phonon addition with the continuous measurement of mechanical amplitude and phase fluctuations. We reconstruct the density matrix of a mechanical oscillator in a phonon-added or phonon-subtracted thermal state with initial mean phonon occupancy of approximately $kT/\hbar\omega_{\mathrm{m}} = 1580$.

Phonon-addition and subtraction arise from the inelastic scattering of laser light due to mechanical motion in a cavity. By energy conservation, photons scattered by mechanical motion are shifted to a lower (higher) frequency corresponding to addition (subtraction) of a phonon in the mechanical resonator (Fig. 1a). For a laser blue-detuned from the optical cavity, the Hamiltonian describing phonon-addition is given by: $\hat{H} = \hbar G(\hat{a}^\dagger\hat{b}^\dagger + h.c.)$ where G is the linearized optomechanical coupling rate, and the annihilation operators for optical and mechanical oscillators are given by $\hat{a}$ and $\hat{b}$ respectively. Similarly, for red-detuning we have $\hat{H} = \hbar G(\hat{a}^\dagger\hat{b} + h.c.)$ whereby a phonon is annihilated while a photon is generated. In our experiments, the optical cavity decay rate κ is much faster than G, and its photons are sent to a detector. Instead of coherent dynamics between the optical field and motion, detection leads to a quantum operation with corresponding jump operators proportional to $\hat{b}^\dagger$ and $\hat{b}$ for the two Hamiltonians, respectively. Therefore, the detection of an individual photon at the cavity resonance frequency heralds the addition or subtraction of a phonon to the mechanical mode characterized by the operation of the respective jump operator. The state of the mechanical oscillator will be thermal before the record of detections is taken into account. This reflects our lack of knowledge about the motional state and that the mechanical oscillator is in equilibrium with its environment. Starting with the thermal density matrix $\hat{\rho}_{\mathrm{th}}$, detection of a photon corresponds to updating the state with the jump operator corresponding to the correct detuning. For the blue-detuned case, we use the jump oper-

* rishipat@stanford.edu
† safavi@stanford.edu

ator proportional to $\hat{b}^\dagger$ to obtain the phonon-added state: $\hat{\rho}_{\text{th}} \rightarrow \hat{b}^\dagger \hat{\rho}_{\text{th}} \hat{b}$. In the red-detuned case, we have phonon-subtraction represented by: $\hat{\rho}_{\text{th}} \rightarrow \hat{b} \hat{\rho}_{\text{th}} \hat{b}^\dagger$.

Our experimental setup is shown in simplified form in Fig.1b. First, we send light from a laser into an optomechanical crystal cavity, either red-detuned or blue-detuned from the cavity resonance by the mechanical frequency. The fiber to chip coupling efficiency is $\eta_{\text{f}} \approx 76\,\%$. The fiber-coupler design and optimization is described in previous work [29]. We split off some of the light before interacting with the device, to use as a local oscillator. A delay is applied using about 100 meters of fiber to approximately compensate for the signal path. A continuous wave, frequency upshifted (40 MHz), probe tone is generated using an acousto-optic-modulator. The reflected light from the cavity is then split into two paths. One path, for single photon counting, contains two cascaded high finesse fiber fabry-perot cavity filters with free spectral range of 15 GHz and finesse of 300 (Micron Optics FFP-I) to suppress the pump light and pass resonant cavity photons. Another path, for heterodyne detection, contains a balanced heterodyne receiver (Thorlabs 75 MHz PDB425C-AC) whose output is sent to a 12 bit 500 MS s^{-1} digitizer (Alazartech ATS 9350). The local oscillator and signal are combined on a variable optical coupler to balance power on the detector inputs. We note that the phase of our local oscillator is left unlocked. This simplifies the experiment but at the cost of causing our inferred states to have rotationally symmetric quasi-probability distributions. Note that the initial state is a rotationally symmetric thermal state, and that the photon addition and subtraction processes occur at random times and have no associated phase.

To count single photons we use a superconducting nanowire single photon detector (SNSPD, Photon Spot) with an effective quantum efficiency of about 70 % (including all fiber losses leading into the fridge) and dark counts on the order of 30 Hz.

Our optomechanical crystal device, used to read out and control mechanical motion, is similar to those presented in previous work [30]. The optical cavity mode has a center wavelength of $\lambda_{\text{c}} = 1551\,\text{nm}$, total decay rate $\kappa/2\pi = 822\,\text{MHz}$, and external coupling rate of $\kappa_{\text{e}}/2\pi = 190\,\text{MHz}$. The probability that a cavity photon leaks into the detected waveguide channel is given by the cavity efficiency, $\eta_{\text{c}} = \kappa_{\text{e}}/\kappa \approx 23\,\%$. The mechanical mode frequency is $\omega_{\text{m}}/2\pi \approx 3.96\,\text{GHz}$. From a sweep of laser power, we determine the intrinsic, backaction-free, mechanical linewidth of $\gamma_{\text{i}}/2\pi = (2.06 \pm 0.01)\,\text{MHz}$ and single-photon optomechanical coupling rate $g_0/2\pi = (1.01 \pm 0.02)\,\text{MHz}$. The single-photon generation rate per phonon in the mechanical resonator is proportional to the optomechanical measurement rate: $\gamma_{\text{OM}} = 4g_0^2 n_{\text{cav}}/\kappa$, where n_{cav} is the number of optical intracavity photons (on order 10^2 in this experiment).

The first experiment we perform is phonon-addition. We tune the laser on the blue side of the optical cavity resonance. We trigger the digitizer on a single photon click, collect $\approx 2\,\mu\text{s}$ of heterodyne data, and filter to obtain a signal whose in-phase (X) and in-quadrature (P) components are proportional to the down-converted mechanical signal. We collect data in two interleaved phases, one ignoring, and the other triggered by single photon clicks. When the clicks are ignored, we observe a Gaussian quadrature histogram, corresponding to a mechanical thermal state, over a total period of $\approx 2\,\text{h}$ (Fig. 2a). By contrast, triggering via single photon clicks, we observe a clear non-Gaussian distribution in the phonon-added thermal state in Fig. 2b.

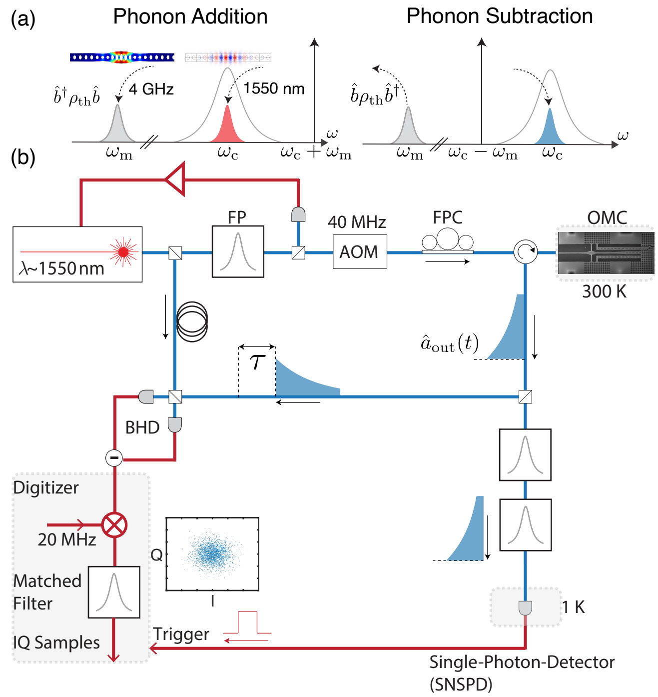

FIG. 1. **Concept and principal components of the experimental setup** (a) Concept showing on left (right) how a Raman scattered photon on cavity-resonance at frequency ω_{c} heralds the addition (subtraction) of a phonon at the mechanical frequency ω_{m}. Insets from left to right show simulated mechanical and optical mode profiles respectively. (b) Diagram showing the main components of the setup. A tunable laser is stabilized to a Fabry-Perot cavity (FP) and is frequency upshifted using an acousto-optic modulator (AOM). The resulting signal polarization is set using a fiber polarization controller (FPC) and sent into the optomechanical crystal device (OMC) whose temperature is stabilized near 300 K. The reflected light is incident on a beamsplitter and is split into two paths. On the bottom, we reject pump light with two FP filers, followed by single photon detection using a superconducting nanowire single photon detector (SNSPD). To the left, we perform balanced heterodyne detection (BHD) where the resulting signal is further digitally downconverted from 20 MHz, and filtered using a digitizer and GPU. A schematic of the decaying cavity field is shown inset in the figure. τ denotes the time-lag between when the click occurs and when the heterodyne data collection starts.

The Husimi Q function for the post-selected phonon-added thermal state has the form:

$$Q_{\text{post}}(\alpha) \propto \langle\alpha|\,\hat{b}^{\dagger}\hat{\rho}_{\text{th}}\hat{b}\,|\alpha\rangle \propto |\alpha|^{2}e^{-|\alpha|^{2}/(\bar{n}_{\text{th}}+1)}, \qquad (1)$$

where $\bar{n}_{\text{th}}$ is the mean thermal phonon occupancy and $|\alpha\rangle$ denotes a coherent state with complex amplitude $\alpha = X + iP$. $Q_{\text{post}}(\alpha)$ describes the measurement statistics in phase space, in the absence of technical noise. The effect of technical noise is captured by convolving this Q function with a Gaussian distribution $\mathcal{N}$, with zero mean and a variance of n_{added}:

$$Q(\alpha) = \Big(Q_{\text{post}} * \mathcal{N}\Big)(\alpha). \qquad (2)$$

(See Supplementary Information [31] for an analytic expression for the measured $Q(\alpha)$ which depends only on $\bar{n}_{\text{th}}$ and n_{added}). This distribution is binned, and fit to the data via a maximum-likelihood method. Since the bath temperature is known ($T \approx 300\,\text{K}$), we fix $\bar{n}_{\text{th}} = 1578$ in Eq. 1 and fit Eq. 2 via two free parameters: detection gain G, and number of added noise phonons n_{added}. The parameter G is used to re-scale the data as $v = \sqrt{G}\alpha$. The result of the fit with $(G, n_{\text{added}}) = (8.1\times10^{-3}\ \text{V}^2, 670)$ is shown in Fig. 2c,d, in good agreement with the experimental results of Fig. 2a,b for both pre- and post-selected distributions. We note that the thermal datasets are interleaved with the post-selection data sets to mitigate the effects of drift. Furthermore, no additional fitting is performed on the thermal datasets, confirming the validity of our gain and added noise estimates. Figure 2e shows a line-cut of the 2D histograms with fit results for the thermal (solid line) and post-selected (dotted line) distributions respectively.

To more compactly represent the data, we bin it into a radial histogram. The results of radial binning for the thermal and phonon-added states are shown in (Fig. 3a). Here, blue (red) points show thermal (phonon-added) results respectively, while the dotted lines show the theoretical fits. In addition, we perform phonon-subtraction by tuning our pump laser to the red side of the optical cavity. The radial statistics for the resulting noise distribution is shown by the open green triangles. As expected from theory, the result is very similar to the case of phonon-addition.

To further analyze the data, we reconstruct the density matrix describing the mechanical system. From the radial histograms, we estimate the density matrix using an iterative maximum-likelihood method [32, 33]. We simplify the optimization by restricting ourselves to diagonal density matrices, as justified by the radial symmetry of the phase space distribution (see Supplementary Information for a complete discussion of these techniques). The results are shown in Fig. 3b. From this reconstruction, we obtain a mean phonon number of $\bar{n}_{\text{th}} = 1597.6 \pm 0.6$ and $\bar{n}_{\text{post}} = 3158.1 \pm 0.9$ for the thermal and post-selected states respectively. The probability of the vacuum component is reduced markedly post-addition of a phonon, going from $p_{\text{vac,th}} = (6.49 \pm 0.01) \times 10^{-4}$ to $p_{\text{vac,post}} = (5.25 \pm 0.06) \times 10^{-5}$. Errors reflect statistical uncertainty obtained using a bootstrapping method of the entire dataset: we resample the entire dataset of 1.5×10^{7} samples with replacement 50 times, and reconstruct the density matrix for each trial. Lastly, we perform the reconstruction of the phonon-subtracted state (Fig. 3c), where we find $\bar{n}_{\text{post}} = 3153.5 \pm 1.0$.

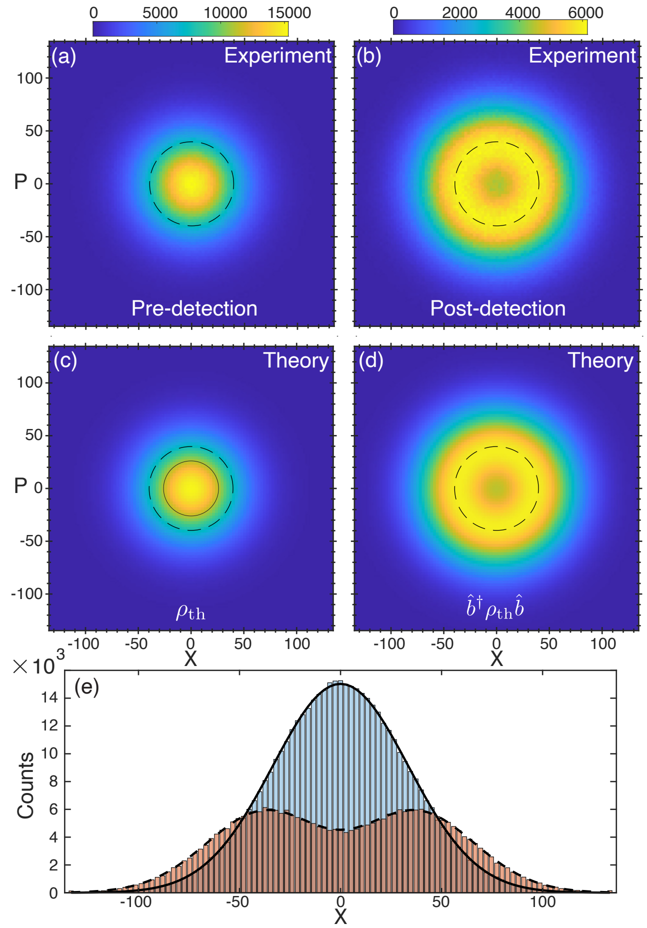

FIG. 2. **Measurement of quadrature histograms for thermal and phonon-added thermal state** (a) Experimental result showing a histogram of 1.5×10^{7} quadrature samples. The data are binned into 101 bins along the X and P axes. Color bars show counts per bin. The statistics are Gaussian, corresponding to a mechanical thermal state. (b) Post-selected results, triggered by single-photon clicks. The observed statistical distribution now corresponds to a phonon-added state and is non-Gaussian. (c,d) Corresponding theory plots to (a,b), obtained by binning, and fitting, the analytically determined Husimi Q functions via two parameters. The dotted black circles, shown for reference, have radii $r = \sqrt{\bar{n}_{\text{th}}}$, the length scale for thermal fluctuations. $\bar{n}_{\text{th}} \approx 1580$ phonons, corresponding to the mean occupancy of a 3.96 GHz oscillator at room temperature. The solid black circle shows the length scale for added noise. (e) Blue (red) bars correspond to a linecut of the 2D experiment histograms at $P = 0$ for the thermal (post-selected) datasets. The theory fits for the thermal (post-selected) results are shown in solid (dotted) black lines.

Next, we use our reconstruction results to investigate how the expected number of phonons changes after post-selection. We compute the ratio of the two mean phonon numbers as $\bar{n}_{\rm post}/\bar{n}_{\rm th} = 1.977 \pm 0.001$. This is in agreement with theory, in which the mean phonon number for both the phonon-added and -subtracted thermal states should approximately be twice that of the original thermal state. This counter-intuitive result that adding *or* subtracting a phonon *doubles* the mean number of phonons in a resonator, $\bar{n}_{\rm post} \approx 2\bar{n}_{\rm th}$, is best understood by considering the information gained about the mechanical system from the optical single photon measurement. Before the measurement of a photon occurs, the *a-priori* probability distribution is given by the Boltzmann factor: $P(n) \propto e^{-\beta n}$ where β is the inverse temperature (Fig. 3b, blue curve). Once a click has occurred however, the observer gains information about the state, and we must update these probabilities via Bayes' rule: $P(n|\text{det}) \propto P(\text{det}|n)P(n)$, causing a rescaling of the *a-priori* distribution. Now, the probability of a photon scattering event itself depends on the phonon number: $P(\text{det}|n) \propto n$. Thus we see that the *a-posteriori* probability is the prior distribution re-scaled by n, leading to the suppression of probability for small phonon numbers (Fig. 3b). This causes the average phonon number to be increased. This analysis, while illustrated for phonon-addition, applies as well to phonon-subtraction in the large thermal occupation limit (see Supplementary Information Eq. S4).

We understand the small discrepancy with the theory prediction of an exact doubling in mean phonon number by considering dark counts. Dark counts introduce a loss in fidelity of the heralded state. More precisely, the heralding fidelity is defined by the quantity $\chi = \Gamma_{\rm sig}/(\Gamma_{\rm sig} + \Gamma_{\rm dark})$. Here, $\Gamma_{\rm sig}$ denotes the count rate of thermal signal phonons, while $\Gamma_{\rm dark}$ denotes the total dark count rate, caused by a sum of intrinsic SNSPD dark counts and pump feedthrough from imperfect pump rejection filtering. We have independently estimated these quantities, using the measured photon count rate on-resonance, and off-resonance. We measure $\Gamma_{\rm sig} \approx (278 \pm 5)\,\text{kHz}$ and $\Gamma_{\rm dark} \approx (5.2 \pm 0.1)\,\text{kHz}$. From this we estimate the fidelity, $\chi \approx 0.98 \pm 0.02$. Written in terms of fidelity, the theoretically expected ratio of mean occupancy is: $\bar{n}_{\rm post}/\bar{n}_{\rm th} \approx 1 + \chi$. The measured fidelity χ thus closely explains the observed ratio $\bar{n}_{\rm post}/\bar{n}_{\rm th}$.

In this work we have experimentally demonstrated phonon addition and subtraction followed by state tomography in an optomechanical system. These capabilities open up several directions for future studies. First of all, the single-phonon-added thermal states demonstrated here have theoretically been shown to be non-classical at all temperatures. This is ensured by the negativity of their Glauber-Sudarshan P functions [16, 19, 34]. Although this negativity is difficult to detect experimentally at room temperature, our work motivates further studies into whether weakly non-classical, but non-Gaussian, states may prove useful as a quantum resource [35, 36]. Finally, our experiment demonstrates the ability to add a node to the Q function of a single-mode oscillator. Since it is known that any pure state whose Q function contains nodes is non-classical [37], one could prepare non-classical states beyond the phase insensitive ones we have reconstructed. In particular, with near-term improvements, including the implementation of phase-sensitive detection, our technique allows the preparation of phonon-added coherent states of motion [38, 39]. Likewise, phonon-subtraction, performed on a squeezed mechanical steady state, gives a route to cat state generation in the mechanical domain [12, 40].

During the preparation of this manuscript we became aware of related work demonstrating variance doubling in phonon-added and subtracted mechanical thermal states [8].

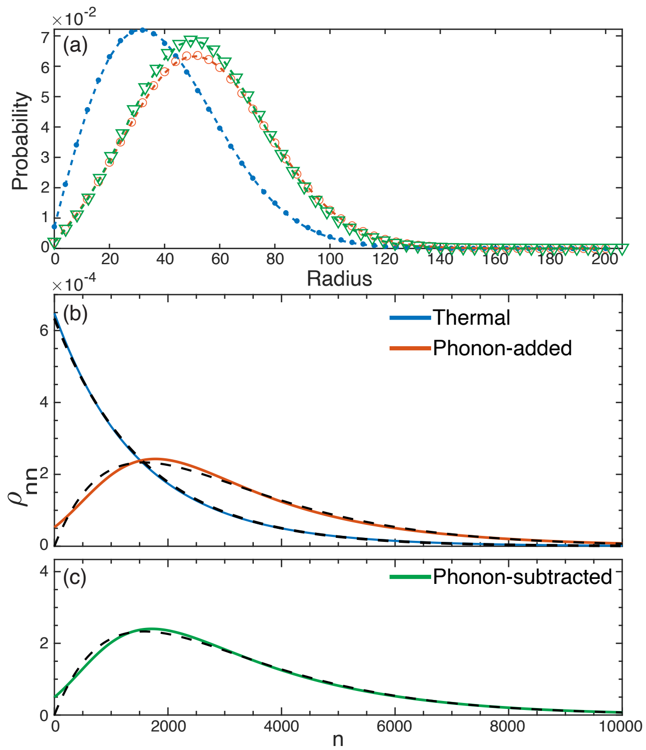

FIG. 3. **Reconstructed density matrix elements** (a) Radial histogram of measurement results for the thermal state (filled blue points), the phonon-added thermal state (open red circles) and the phonon-subtracted thermal state (green triangles). The respective dotted lines show the theory fits. (b) Diagonal density matrix elements reconstructed from experimental data. Estimates for gain and added noise are provided by the fits to the quadrature histogram data. The black dotted lines show the result of theory for the thermal and phonon-added states with thermal bath occupancy set to $\bar{n}_{\rm th} = 1578$ phonons ($\approx 300\,\text{K}$ mode temperature). (c) Experimentally reconstructed density matrix elements for a phonon-subtracted thermal state.

ACKNOWLEDGMENTS

This work was funded by the U.S. government through the Department of Energy through Grant No. DE-SC0019174, and the U.S. Army Research Office (ARO)/Laboratory for Physical Sciences (LPS) Cross-Quantum Systems Science & Technology (CQTS) program (Grant No. W911NF-18-1-0103). The authors wish to thank NTT Research for their financial and technical support. We acknowledge the David and Lucille Packard Fellowship, and the Stanford University Terman Fellowship. We thank Pieter-Jan C. Stas, Alex Wollack, Hubert Stokowski and Marek Pechal for experimental support. Device fabrication was performed at the Stanford Nano Shared Facilities (SNSF) and the Stanford Nanofabrication Facility (SNF). The SNSF is supported by the National Science Foundation under Grant No. ECCS-2026822. RNP was partly supported by the National Science Foundation Graduate Research Fellowship under Grant No. DGE-1656518.

[1] J. I. Cirac and P. Zoller, Physical review letters **74**, 4091 (1995).

[2] T. P. Purdy, K. E. Grutter, K. Srinivasan, and J. M. Taylor, Science **356**, 1265 (2017).

[3] V. Sudhir, D. J. Wilson, R. Schilling, H. Schütz, S. A. Fedorov, A. H. Ghadimi, A. Nunnenkamp, and T. J. Kippenberg, Physical Review X **7**, 11001 (2017).

[4] T. A. Palomaki, J. D. Teufel, R. W. Simmonds, and K. W. Lehnert, Science **342**, 710 (2013).

[5] J. D. Cohen, S. M. Meenehan, G. S. MacCabe, S. Gröblacher, A. H. Safavi-Naeini, F. Marsili, M. D. Shaw, and O. Painter, Nature **520**, 522 (2015).

[6] R. Riedinger, S. Hong, R. A. Norte, J. A. Slater, J. Shang, A. G. Krause, V. Anant, M. Aspelmeyer, and S. Gröblacher, Nature **530**, 313 (2016), arXiv:1512.05360.

[7] R. Riedinger, A. Wallucks, I. Marinković, C. Löschnauer, M. Aspelmeyer, S. Hong, and S. Gröblacher, Nature **556**, 473 (2018).

[8] G. Enzian, J. J. Price, L. Freisem, J. Nunn, J. Janousek, B. C. Buchler, P. K. Lam, and M. R. Vanner, Physical Review Letters **126**, 33601 (2021).

[9] E. J. Davis, Z. Wang, A. H. Safavi-Naeini, and M. H. Schleier-Smith, Physical Review Letters **121**, 123602 (2018).

[10] S. T. Velez, K. Seibold, N. Kipfer, M. D. Anderson, V. Sudhir, and C. Galland, Physical Review X **9**, 041007 (2019), arXiv:1811.03038.

[11] A. I. Lvovsky, H. Hansen, T. Aichele, O. Benson, J. Mlynek, and S. Schiller, Physical Review Letters **87**, 50402 (2001), arXiv:0101051 [quant-ph].

[12] A. Ourjoumtsev, R. Tualle-Brouri, J. Laurat, and P. Grangier, Science **312**, 83 (2006).

[13] D. V. Sychev, A. E. Ulanov, A. A. Pushkina, M. W. Richards, I. A. Fedorov, and A. I. Lvovsky, Nature Photonics **11**, 379 (2017).

[14] A. I. Lvovsky, P. Grangier, A. Ourjoumtsev, V. Parigi, M. Sasaki, and R. Tualle-Brouri, arXiv preprint arXiv:2006.16985 (2020).

[15] A. Zavatta, V. Parigi, M. S. Kim, H. Jeong, and M. Bellini, Physical Review Letters **103**, 140406 (2009).

[16] T. Kiesel, W. Vogel, V. Parigi, A. Zavatta, and M. Bellini, Physical Review A - Atomic, Molecular, and Optical Physics **78** (2008), 10.1103/PhysRevA.78.021804, arXiv:0804.1016.

[17] T. Kiesel, W. Vogel, M. Bellini, and A. Zavatta, Physical Review A - Atomic, Molecular, and Optical Physics **83** (2011), 10.1103/PhysRevA.83.032116, arXiv:1101.1741.

[18] M. D. Vidrighin, O. Dahlsten, M. Barbieri, M. S. Kim, V. Vedral, and I. A. Walmsley, Physical Review Letters **116** (2016), 10.1103/PhysRevLett.116.050401, arXiv:1510.02164.

[19] A. Zavatta, V. Parigi, and M. Bellini, Physical Review A - Atomic, Molecular, and Optical Physics **75** (2007), 10.1103/PhysRevA.75.052106.

[20] V. Parigi, A. Zavatta, M. Kim, and M. Bellini, Science **317**, 1890 (2007), arXiv:arXiv:1308.5367.

[21] A. D. O'Connell, M. Hofheinz, M. Ansmann, R. C. Bialczak, M. Lenander, E. Lucero, M. Neeley, D. Sank, H. Wang, M. Weides, J. Wenner, J. M. Martinis, and A. N. Cleland, Nature **464**, 697 (2010), arXiv:1602.03841.

[22] Y. Chu, P. Kharel, T. Yoon, L. Frunzio, P. T. Rakich, and R. J. Schoelkopf, Nature **563**, 666 (2018), arXiv:1804.07426.

[23] K. J. Satzinger, Y. P. Zhong, H. S. Chang, G. A. Peairs, A. Bienfait, M. H. Chou, A. Y. Cleland, C. R. Conner, Dumur, J. Grebel, I. Gutierrez, B. H. November, R. G. Povey, S. J. Whiteley, D. D. Awschalom, D. I. Schuster, and A. N. Cleland, Nature **563**, 661 (2018), arXiv:1804.07308.

[24] P. Arrangoiz-Arriola, E. A. Wollack, Z. Wang, M. Pechal, W. Jiang, T. P. McKenna, J. D. Witmer, R. Van Laer, and A. H. Safavi-Naeini, Nature **571**, 537 (2019).

[25] A. I. Lvovsky and M. G. Raymer, Reviews of Modern Physics **81**, 299 (2009), arXiv:0511044 [quant-ph].

[26] C. Eichler, D. Bozyigit, C. Lang, L. Steffen, J. Fink, and A. Wallraff, Physical Review Letters **106**, 220503 (2011).

[27] M. R. Vanner, J. Hofer, G. D. Cole, and M. Aspelmeyer, Nature Communications **4**, 1 (2013).

[28] J. T. Muhonen, G. R. L. Gala, R. Leijssen, and E. Verhagen, Physical Review Letters **123**, 113601 (2019).

[29] R. N. Patel, Z. Wang, W. Jiang, C. J. Sarabalis, J. T. Hill, and A. H. Safavi-Naeini, Physical Review Letters **121**, 40501 (2018), arXiv:1711.00847.

[30] R. N. Patel, C. J. Sarabalis, W. Jiang, J. T. Hill, and A. H. Safavi-Naeini, Physical Review Applied **8**, 1 (2017), arXiv:1705.07869.

[31] See Supplementary Information which includes [41–44].

[32] A. I. Lvovsky, Journal of Optics B: Quantum and Semiclassical Optics **6**, S556 (2004).

[33] C. Eichler, D. Bozyigit, and A. Wallraff, Physical Review A **86**, 32106 (2012).

[34] G. S. Agarwal and K. Tara, Physical Review A **46**, 485 (1992).

[35] Q. Zhuang, P. W. Shor, and J. H. Shapiro, Physical Review A **97**, 052317 (2018), arXiv:1803.07580.

[36] M. G. Genoni, M. L. Palma, T. Tufarelli, S. Olivares, M. S. Kim, and M. G. Paris, Physical Review A - Atomic, Molecular, and Optical Physics **87**, 062104 (2013), arXiv:1304.3340.

[37] U. Chabaud, D. Markham, and F. Grosshans, Physical Review Letters **124**, 63605 (2020).

[38] J. Li, S. Gröblacher, S.-Y. Zhu, and G. S. Agarwal, Physical Review A **98** (2018), 10.1103/PhysRevA.98.011801.

[39] G. S. Agarwal and K. Tara, Physical Review A **43**, 492 (1991).

[40] A. Kronwald, F. Marquardt, and A. A. Clerk, Physical Review A **88**, 063833 (2013).

[41] A. H. Safavi-Naeini, J. Chan, J. T. Hill, S. Gröblacher, H. Miao, Y. Chen, M. Aspelmeyer, and O. Painter, New Journal of Physics **15** (2013), 10.1088/1367-2630/15/3/035007, arXiv:1210.2671.

[42] F. Y. Khalili, H. Miao, H. Yang, A. H. Safavi-Naeini, O. Painter, and Y. Chen, Physical Review A **86**, 033840 (2012).

[43] J. Řeháček, Z. Hradil, E. Knill, and A. I. Lvovsky, Physical Review A - Atomic, Molecular, and Optical Physics **75**, 1 (2007), arXiv:0611244 [quant-ph].

[44] C. Eichler, *Experimental characterization of quantum microwave radiation and its entanglement with a superconducting qubit*, Ph.D. thesis, ETH Zurich (2013).